

A High Order Sharp-Interface Method with Local Time Stepping for Compressible Multiphase Flows

Angela Ferrari^{1,*}, Claus-Dieter Munz¹ and Bernhard Weigand²

¹ Institute of Aerodynamics and Gasdynamics, University of Stuttgart,
Pfaffenwaldring 21, D-70569 Stuttgart, Germany.

² Institute of Aerospace Thermodynamics, University of Stuttgart,
Pfaffenwaldring 31, D-70569 Stuttgart, Germany.

Received 9 March 2010; Accepted (in revised version) 5 May 2010

Available online 5 August 2010

Abstract. In this paper, a new sharp-interface approach to simulate compressible multiphase flows is proposed. The new scheme consists of a high order WENO finite volume scheme for solving the Euler equations coupled with a high order path-conservative discontinuous Galerkin finite element scheme to evolve an indicator function that tracks the material interface. At the interface our method applies ghost cells to compute the numerical flux, as the ghost fluid method. However, unlike the original ghost fluid scheme of Fedkiw et al. [15], the state of the ghost fluid is derived from an approximate-state Riemann solver, similar to the approach proposed in [25], but based on a much simpler formulation. Our formulation leads only to one single *scalar* nonlinear algebraic equation that has to be solved at the interface, instead of the *system* used in [25]. Away from the interface, we use the new general Osher-type flux recently proposed by Dumbser and Toro [13], which is a simple but *complete* Riemann solver, applicable to general hyperbolic conservation laws. The time integration is performed using a fully-discrete one-step scheme, based on the approaches recently proposed in [5, 7]. This allows us to evolve the system also with time-accurate local time stepping. Due to the sub-cell resolution and the subsequent more restrictive time-step constraint of the DG scheme, a local evolution for the indicator function is applied, which is matched with the finite volume scheme for the solution of the Euler equations that runs with a larger time step. The use of a locally optimal time step avoids the introduction of excessive numerical diffusion in the finite volume scheme. Two different fluids have been used, namely an ideal gas and a weakly compressible fluid modeled by the Tait equation. Several tests have been computed to assess the accuracy and the performance of the new high order scheme. A verification of our algorithm has been carefully carried out using exact solutions as well as a comparison with other numerical reference solutions. The material interface is resolved sharply and accurately without spurious oscillations in the pressure field.

*Corresponding author. *Email addresses:* iagferra@iag.uni-stuttgart.de (A. Ferrari), munz@iag.uni-stuttgart.de (C.-D. Munz), bernhard.weigand@itlr.uni-stuttgart.de (B. Weigand)

AMS subject classifications: 76T10, 65M08, 65M60

Key words: Sharp interface capturing, compressible multiphase flows, one-step time-integration, time-accurate local time stepping, modified ghost fluid method, WENO schemes, discontinuous Galerkin methods.

1 Introduction

The simulation of compressible multiphase problems, such as reactive flows in combustion processes or flows involving phase changes, introduces many numerical difficulties associated with the treatment of the material interface. Numerical inaccuracies and spurious oscillations can occur at contact discontinuities even if diffusion and chemical reactions are not considered. In particular, unphysical oscillations in the pressure field arise at the material interface due to the change of the equation of state and the large density gradients across the interface, in particular in the case of simulations of fluids involving liquids and gases.

Different approaches have been proposed in literature. For mixtures of perfect gases with a non-constant ratio of specific heats, Abgrall [1] developed a successful quasi-conservative approach. However, the approach is limited to mixtures of ideal gases so far. A simple correction of the total energy has been proposed by Jenny et al. [22] computing the in-and outgoing volume fluxes over each cell interface such that a constant pressure in all fluids is achieved by decoding the conservative variables from the numerical fluxes. Although the numerical approaches just mentioned are successful for specific test cases, it is hard to extend them to more complex applications that contain gases and liquids with other *general* equations of state.

A completely different treatment of the material interface consists of tracking it explicitly with a level set function [27, 33], which is a signed distance function that takes the value zero at the interface. Fedkiw et al. [14, 15] proposed the well-known ghost fluid method that reduces the problem of interactions of two different fluids at the material interface to two separate single-phase Riemann problems. The missing values for density, velocity and pressure on the other side of the material interface are assigned to a *ghost fluid* by a suitable procedure based on one sided extrapolation of the entropy, described in detail in [15]. This method simulates properly and efficiently general compressible multiphase flow problems avoiding spurious oscillations in the pressure and density fields at the material interface. However, Liu et al. showed from a complete analysis in [25] that the original ghost fluid method does not work correctly when applied to a strong shock impacting on a material interface, because the locations of the shock front and interface are computed in a wrong manner. Liu et al. [25] provided an improved ghost fluid method, in which a nonlinear algebraic system at the interface is solved at the interface position. It is derived from a two-shock approximation to the Riemann problem at the interface and is written for the general Mie-Grüneisen family of equations of state. The

resulting algorithm is able to cure the main deficiencies inherent in the original ghost fluid approach.

Another method to track material interfaces is the volume of fluid (VOF) method, which has been introduced by Hirt and Nichols in [20]. It is based on the concept of a fractional volume of fluid and defines a function whose value is unity at any point occupied by one fluid and zero otherwise. This function moves with the fluid and a non-conservative evolution equation is used to evolve it. However, up to now, most of the applications of the VOF method are restricted to the simulation of incompressible fluids.

Chang and Liou [3,24] introduced a new diffuse-interface method based on an extension of the AUSM⁺ scheme to solve compressible multiphase flows. It is based on the *stratified* flow approach, where the interactions of fluids of the same type are computed by a traditional method for the solution of hyperbolic conservation laws. The computation of interactions of fluids of different type require the exact or approximate solution of the corresponding multi-phase Riemann problem. Additional dissipation terms have been added to the AUSM⁺ flux to apply the scheme to both liquid and gas flows. Although the dissipation terms actually enhance the stability of the scheme, it can occur in some pathological situations that the system of equations becomes ill-posed, i.e., that hyperbolicity is lost, see [3].

In this paper, we propose a new sharp-interface method. The interface is identified by the zero-level of a function whose evolution is governed by a non-conservative advection equation that is solved with a path-conservative approach [30], based on a high order accurate path-conservative discontinuous Galerkin (DG) finite element (FE) method [6, 8, 32]. The use of a high order DG scheme [4] allows us to track the material interface very accurately with a sub-cell resolution. In our approach, the compressible Euler equations are solved with a high order accurate finite volume scheme based on the WENO reconstruction of Dumbser et al. [7,9,10]. The time integration is performed using an ADER-type (Arbitrary order DERivative Riemann problem) time stepping procedure, introduced for conservation laws by Titarev and Toro [34, 36, 37] and subsequently generalized by Dumbser et al. [6, 8] to non-conservative hyperbolic systems. Since the DG scheme has a more restrictive time step than the finite volume scheme due to the linear stability condition, a time-accurate local time stepping [11, 18] has been introduced in the new method to obtain a significant improvement in the computational performance with respect to a global time stepping scheme and also to reduce the numerical diffusion in the WENO FV scheme for the Euler equations, because this corresponds to increase the Courant number. This is an essential feature for a future extension to multiple space dimensions. The interactions over the material interface are computed using the ghost fluid approach, since it can be easily applied to general equations of state. However, instead of using one sided extrapolation of the entropy to define the state of the ghost cells as Fedkiw et al. [15], we solve Riemann problems at the interface using an approximate-state Riemann solver, as first proposed by Liu et al. [25]. However, our algorithm is considerably simpler in comparison with the approach of Liu et al. [25], that requires the solution of a 6×6 nonlinear algebraic system. Our method reduces the effort to the solution of only

one single scalar nonlinear algebraic equation. In this paper, we model the gas phase as an ideal gas and the liquid phase is modeled as a weakly compressible fluid governed by the Tait equation of state. Several numerical test cases have been solved to assess the accuracy and the performance of the new high order scheme by comparing against exact or numerical reference solutions.

In what follows, we consider the physical model in Section 2, i.e., the compressible one-fluid Euler equations for two fluids, which are separated by a material interface. The interface is tracked by a non-conservative evolution equation for an indicator function. In Section 3, the new numerical scheme is explained. First, the focus is on the definition of the ghost states across the material interface and second, the WENO reconstruction for the solution of the Euler equations is briefly described. Afterwards, Section 3.4 regards the time integration using the ADER-type one-step approach together with the local time stepping, applied to the evolution of the indicator function by the path-conservative DG method. The numerical results are presented in Section 4 and good accuracy is obtained applying the new approach. Conclusions and an outlook to future work are presented in Section 5.

2 Physical model

The basic equations governing compressible one-dimensional flows consist of the Euler equations

$$\frac{\partial Q}{\partial t} + \frac{\partial F(Q)}{\partial x} = 0, \quad (2.1)$$

with the vector of conserved variables Q and the flux vector F being defined as

$$Q = \begin{pmatrix} \rho \\ \rho v \\ \rho e \end{pmatrix}, \quad F = \begin{pmatrix} \rho v \\ \rho v^2 + p \\ v(\rho e + p) \end{pmatrix}. \quad (2.2)$$

Here, t is time, x is the spatial coordinate, ρ is the density, v is the velocity, e is the total energy per unit mass and p is the pressure. To simulate a multifluid system the variables in Eq. (2.2) are related to one sort of fluid (gas or liquid) in each cell. In this paper, the fluids are assumed chemically non-reacting, not in equilibrium and they do not inter-penetrate. They interact over the contact interface that is marked using an indicator function f . It is a numerical function, whose positive values correspond to one fluid and the negative values correspond to the other. The zero level of the indicator function marks the location of the material discontinuity. The temporal evolution of the indicator function is performed solving the following partial differential equation (PDE) in non-conservative form

$$\frac{\partial f}{\partial t} + v \frac{\partial f}{\partial x} = 0. \quad (2.3)$$

Eq. (2.3) corresponds to the evolution equation of the level set function used by Fedkiw et al. [15]. Here, we use for simplicity an indicator function for which it is much easier to

determine the initial conditions: constant states on the left and right sides of the interface are assigned according to the type of the fluid. Note that no positivity condition must be guaranteed unlike the mass/volume fraction function of the VOF method, but given Eq. (2.3) each fluid is defined by the value of the indicator function. The discretization of Eq. (2.3) can be done independently of the set of Euler equations (2.1).

In our applications, two different equations of state (EOS) have been used. The gas component has been modeled by the EOS of an ideal gas

$$p = (\gamma_G - 1) \left(\rho e - \frac{1}{2} \rho v^2 \right), \quad (2.4)$$

where γ_G denotes the ratio of specific heats. The liquid has been modeled as a weakly compressible fluid by the Tait EOS

$$p = k_0 \left[\left(\frac{\rho}{\rho_0} \right)^{\gamma_L} - 1 \right] + p_0, \quad k_0 = \frac{\rho_0}{\gamma_L} \frac{|v|^2}{M^2}, \quad (2.5)$$

where the coefficient k_0 depends on the Mach number M that determines the compressibility of the fluid. Here, $|v|$ is the maximum estimated value of the fluid velocity. The exponent γ_L is constant, usually equal to 7, ρ_0 and p_0 are the density and the pressure of the fluid at reference conditions.

3 Numerical scheme

Given an interface, it consists of a material discontinuity that defines two separate subdomains, each one corresponds to one fluid or the other. In our scheme, the interactions across the interface are performed using the ghost fluid approach that needs the definition of ghost states in order to apply two separate single-phase Riemann problems. Since the Euler equations require a very robust but though high order accurate *shock capturing* scheme, the third order WENO reconstruction is applied. On the other hand, the main requirement for solving the indicator equation is *spatial resolution*. Shock capturing properties are not required for the indicator function since it only consists of a scalar advection equation with variable coefficients if we consider the velocity field as known from the solution of the Euler equations. The key idea is to apply a different numerical approach, i.e., a high order accurate path-conservative discontinuous Galerkin finite element scheme [6, 8, 32] for the evolution of the indicator function.

The one-step time discretization approach [5–8] used here consists of a local time-space Galerkin predictor and provides the evolution of the reconstructed WENO polynomial data inside each element during one time step. The high order accurate one-step time discretization keeps the scheme very compact and enables us to implement a time-accurate local time stepping, described in detail in Section 3.4. It significantly increases the computational efficiency of the scheme with respect to a global time stepping method.

3.1 Ghost fluid approach

In this section, the ghost fluid approach is briefly described. It has been proposed by Fedkiw et al. in [14, 15] and requires the definition of each fluid at every point in the computational domain in order to update each fluid separately in time. In this way, each grid point contains the state (mass, momentum, and energy) for the real fluid that exists at that point, according to the indicator function and a new "ghost" state for the other fluid that does not really exist at the point, because it is on the other side of the interface. Originally [15] one sided extrapolation of the entropy was used to define the density in the ghost cells, whereas the velocity and pressure were simply copied from the real values. However, as proven by Liu et al. in [25], it fails to predict the correct location of the shock front and interface when a strong shock impacts on the material interface. Liu et al. [25] obtained an improvement solving a 6×6 nonlinear algebraic system at the interface. In our scheme, the ghost state is defined through an approximate-state Riemann solver that leads to one simple scalar nonlinear algebraic equation reducing the effort to the solution. The solution of the Riemann problem at the interface is provide via an iterative method after some steps using the shock approximation for the ideal gas and the rarefaction wave approximation for the Tait equation. For details see the Appendix. Once the ghost cells are defined, one can use standard one-phase methods to update the Euler equations at every grid point.

3.2 High order WENO finite volume scheme for the Euler equations

The Euler equations (2.1) are solved using a high order FV scheme based on the WENO reconstruction. The high order reconstruction is achieved using the nonlinear weighted essentially non-oscillatory (WENO) strategy presented in [7, 10], which is different from the original WENO method of Jiang and Shu [23], because it reconstructs entire polynomials instead of point values. It has been implemented in its version with characteristic reconstruction to assure monotonicity at discontinuities also for problems involving strong shock waves. The details on the WENO reconstruction can be found in the three above-mentioned publications. Here, we only give a brief summary of the method.

Integrating the Euler system (2.1) over a space-time control volume $[x_{i-1/2}; x_{i+1/2}] \times [t^n; t^{n+1}]$, we obtain the one-step FV scheme

$$\bar{Q}_i^{n+1} = \bar{Q}_i^n - \frac{\Delta t}{\Delta x} (F_{i+1/2} - F_{i-1/2}), \quad (3.1)$$

where \bar{Q}_i^n denotes the i^{th} cell average at the time step n

$$\bar{Q}_i^{n+1} = \frac{1}{\Delta x} \int_{x_{i-1/2}}^{x_{i+1/2}} Q(x, t^n) dx, \quad (3.2)$$

and $F_{i+1/2}$ is the numerical flux computed at the interface between the cells i and $i+1$,

defined as follows

$$F_{i+\frac{1}{2}} = \int_{t^n}^{t^{n+1}} F_h dt, \quad F_h = F_h\left(Q_{i+\frac{1}{2}}^-(t), Q_{i+\frac{1}{2}}^+(t)\right), \quad (3.3)$$

where F_h is a monotone numerical flux function and the so-called boundary extrapolated values $Q_{i+\frac{1}{2}}^\pm(t)$ are computed with the WENO reconstruction procedure followed by the element local space-time Galerkin predictor, described later. Concerning the numerical flux F_h , we have used the one recently proposed by Dumbser and Toro [13] for non-conservative hyperbolic systems. It represents a *complete* Riemann solver and consists of a generalization of the Osher-Solomon flux [29] to general hyperbolic systems. It reads

$$F_h(Q^-, Q^+) = \frac{1}{2}\left(F(Q^-) + F(Q^+)\right) - \frac{1}{2}\left(\int_0^1 |A(\psi(s))| ds\right)(Q^+ - Q^-), \quad (3.4)$$

with the straight line segment path

$$\psi(s) = Q^- + s(Q^+ - Q^-), \quad 0 \leq s \leq 1, \quad (3.5)$$

and the usual definition of the absolute value of a matrix

$$|A| = R|\Lambda|R^{-1}. \quad (3.6)$$

Here, R denotes the right eigenvector matrix and Λ is a diagonal matrix of corresponding eigenvalues, to which the absolute value operator is applied component wise. The integral appearing in (3.4) is now evaluated approximately using Gauss-Legendre quadrature

$$F_h(Q^-, Q^+) = \frac{1}{2}\left(F(Q^-) + F(Q^+)\right) - \frac{1}{2}\left(\sum_{j=1}^G |A(\psi(s_j))|\right)(Q^+ - Q^-). \quad (3.7)$$

Throughout this article, we use $G=3$ quadrature points.

For the third order WENO scheme used in this article, we first define three reconstruction stencils for each control volume T_i , namely the centered stencil $S_i^0 = \{T_{i-1}, T_i, T_{i+1}\}$, the left-sided stencil $S_i^{-1} = \{T_{i-2}, T_{i-1}, T_i\}$ and the right-sided stencil $S_i^{+1} = \{T_i, T_{i+1}, T_{i+2}\}$. We then compute three different reconstruction polynomials per cell, one obtained for each stencil. The yet unknown coefficients \hat{w}_l of the reconstruction polynomials

$$w_s(x) = \hat{w}_m^s \phi_m(x), \quad (3.8)$$

that use the same basis functions as the DG scheme (3.17) can be obtained by requiring integral conservation of the reconstruction polynomial on the entire stencil s , i.e., we require that

$$\frac{1}{\Delta x} \int_{x_{j-\frac{1}{2}}}^{x_{j+\frac{1}{2}}} w_s(x) dx = \bar{Q}_j, \quad \forall T_j \in S_i^s. \quad (3.9)$$

The final reconstruction polynomial $w_i(x, t^n)$ is then obtained on each control volume T_i by the following WENO procedure

$$w_i(x, t^n) = \sum_{s=-1}^1 \omega_s w_s(x) = \left(\sum_{s=-1}^1 \omega_s \widehat{w}_m^s \right) \phi_m(x), \quad (3.10)$$

with

$$\omega_s = \tilde{\omega}_s \left(\sum_{k=-1}^1 \tilde{\omega}_k \right)^{-1}, \quad \tilde{\omega}_s = \frac{\lambda_s}{(OI_s + \epsilon)^r}, \quad \lambda_s = \begin{cases} 10^6, & \text{if } s=0, \\ 1, & \text{else.} \end{cases} \quad (3.11)$$

We typically choose $\epsilon = 10^{-14}$ and $r = 8$. The oscillation indicators are computed in the classical manner as follows:

$$OI_s = \sum_{\alpha=1}^2 \int_{x_{i-\frac{1}{2}}}^{x_{i+\frac{1}{2}}} \Delta x^{2\alpha-1} \left(\frac{\partial^\alpha \mathcal{W}_s}{\partial x^\alpha} \right)^2 dx. \quad (3.12)$$

3.3 Path-conservative discontinuous Galerkin scheme for the non-conservative indicator equation

The evolution of the indicator function is computed using a high order accurate path-conservative DG scheme [6, 8, 30, 32]. The use of a DG method [4] remarkably increases the accuracy of the numerical solution of the indicator function. This is due to the sub-cell resolution capacity of the DG method in comparison with a classical FV scheme that only evolves cell averages and thus needs a large stencil to reconstruct the function in terms of higher degree polynomials. Due to its higher resolution, the DG method is able to keep initial discontinuities sharper than a finite volume scheme of the same order of accuracy on the same mesh. Actually, in the case of a material interface the initial condition of the indicator function f consists of piecewise constant states on each side of the material interface. For fluid number one the indicator function f takes a positive value and for the second fluid it assumes a negative value. The interface is then defined at the point where the indicator function is zero. Recently, Marchandise et al. [26] have used a quadrature free DG method to solve the level set function on unstructured grids, however without coupling with fluid mechanics yet. They confirm that their DG scheme seems to give more accurate results and to exhibit less mass loss than ENO methods for the level set function.

Benefits come also from the path-conservative approximation. It consists of a generalization of the usual concept of conservative methods for systems of conservation laws and has the property to be automatically conservative, if the evolution equations can be re-written in a conservation form. In our case, this is true when the velocity field in the advection equation (2.3) for the evolution of the indicator function is divergence-free, i.e.,

$$\nabla \cdot v = 0. \quad (3.13)$$

As usual for classical DG schemes [4], we represent the numerical solution at the beginning of a time-step by piecewise polynomials of degree N inside an element as a sum of degrees of freedom \hat{f} and space-only dependent basis functions $\phi = \phi(\xi)$ of maximum degree N as follows

$$f = \sum_{k=0}^N \phi_k(\xi) \hat{f}_k(t) := \phi_k(\xi) \hat{f}_k(t), \quad (3.14)$$

where ξ denotes the local spatial coordinate, i.e.,

$$\xi = \frac{x - x_{i-\frac{1}{2}}}{\Delta x}, \quad (3.15)$$

in the reference coordinate system. Note that the Einstein summation convention has been applied. Multiplying the non-conservative equation (2.3) with test functions ϕ_k and integrating over a space-time control volume

$$T_i = \left[x_{i-\frac{1}{2}}; x_{i+\frac{1}{2}} \right] \times [t^n; t^{n+1}], \quad (3.16)$$

according to the path-conservative approach published in [6,30], we obtain the numerical DG scheme written in semi-discrete form, as follows

$$\begin{aligned} & (\hat{f}_l^{n+1} - \hat{f}_l^n) \int_{x_{i-\frac{1}{2}}}^{x_{i+\frac{1}{2}}} \phi_k \phi_l dx + \int_{t^n}^{t^{n+1}} \int_{x_{i-\frac{1}{2}}}^{x_{i+\frac{1}{2}}} \phi_k \left(v \frac{\partial f}{\partial x} \right) dx dt \\ & + \int_{t^n}^{t^{n+1}} \left(\phi_k^{i+\frac{1}{2}} D_{i+\frac{1}{2}}^- + \phi_k^{i-\frac{1}{2}} D_{i-\frac{1}{2}}^+ \right) dt = 0. \end{aligned} \quad (3.17)$$

The jump terms $D_{i+1/2}^-$ and $D_{i-1/2}^+$ are defined as follows:

$$D_{i+\frac{1}{2}}^- = \frac{1}{2} \left(\tilde{v}_{i+\frac{1}{2}} - \tilde{\lambda}_{\max} \right) \left(f_{i+\frac{1}{2}}^+ - f_{i+\frac{1}{2}}^- \right), \quad \tilde{\lambda}_{\max} = \max \left(|v_{i+\frac{1}{2}}^-|, |v_{i+\frac{1}{2}}^+| \right), \quad (3.18a)$$

$$D_{i-\frac{1}{2}}^+ = \frac{1}{2} \left(\tilde{v}_{i-\frac{1}{2}} + \tilde{\lambda}_{\max} \right) \left(f_{i-\frac{1}{2}}^+ - f_{i-\frac{1}{2}}^- \right), \quad \tilde{\lambda}_{\max} = \max \left(|v_{i-\frac{1}{2}}^-|, |v_{i-\frac{1}{2}}^+| \right), \quad (3.18b)$$

$$\tilde{v}_{i\pm\frac{1}{2}} = \int_0^1 v(\psi(s)) ds = \frac{1}{2} \left(v_{i\pm\frac{1}{2}}^- + v_{i\pm\frac{1}{2}}^+ \right), \quad (3.18c)$$

where $\psi(s)$ denotes the path along which the integral is computed. In our applications, we use the simple segment-path

$$\psi = v_{i+\frac{1}{2}}^- + s \left(v_{i+\frac{1}{2}}^+ - v_{i+\frac{1}{2}}^- \right), \quad 0 \leq s \leq 1. \quad (3.19)$$

In Eq. (3.17), we can assume the velocity field $v = v(x, t)$ as a known function, because it is computed independently by the local space-time Galerkin predictor method for the Euler equations (2.1).

3.4 ADER time integration with local time stepping

Instead of using the governing PDE in its strong differential form to obtain high order of accuracy in time as in the classical ADER approach [10, 12, 34, 36, 37], we resort to the local space-time Galerkin scheme proposed by Dumbser et al. in [5–7] for the time integration. The usual Cauchy Kovalevski procedure used in ADER finite volume schemes developed by Titarev and Toro [34, 36, 37] and the ADER-DG method of Dumbser and Munz [12], Qiu et al. [31] is replaced by a local weak formulation of the governing PDE in space-time. The method proposed in [5] uses a local space-time continuous Galerkin method to predict the evolution of the reconstructed polynomial data $w_i(x, t^n)$ inside each cell during one time step. Thus, high order of accuracy is achieved in a one-step time discretization.

The local space-time Galerkin predictor described in the following evolves the polynomials $w_i(x, t^n)$ given by the WENO reconstruction at time t^n or already defined by the piecewise polynomial data representation of the indicator function f in the discontinuous Galerkin finite element framework. We therefore adopt the notation of Dumbser et al. [5] and define the following two operators

$$\langle A, B \rangle_{T_i} = \int_{t^n}^{t^{n+1}} \int_{T_i} A(x, t) B(x, t) dx dt, \quad (3.20a)$$

$$[A, B]_{T_i}^t = \int_{T_i} A(x, t) B(x, t) dx. \quad (3.20b)$$

They denote the scalar products of two functions A and B over the space-time element $T_i \times [t^n; t^{n+1}]$ and the spatial element T_i , respectively. In the one-dimensional case, the spatial element T_i is $[x_{i-1/2}; x_{i+1/2}]$. The conservation law

$$\frac{\partial Q}{\partial t} + \frac{\partial F(Q)}{\partial x} = 0, \quad (3.21)$$

is now multiplied with a space-time dependent test function $\theta_k = \theta_k(x, t)$ and integration by parts in time is applied to the first term. The numerical solution Q of the previous equation is assumed to be written in terms of the basis functions θ as follows:

$$Q = Q(x, t) = \widehat{Q}_m \theta_m(x, t), \quad (3.22)$$

this yields the following element-local system of algebraic equations

$$[\theta_k, Q]_{T_i}^{t^{n+1}} - \left\langle \frac{\partial}{\partial t} \theta_k, Q \right\rangle_{T_i} + \left\langle \theta_k, \frac{\partial F(Q)}{\partial x} \right\rangle_{T_i} = [\theta_k, w(x, t^n)]_{T_i}^{t^n}, \quad (3.23)$$

that can be easily solved by the fixed-point iteration scheme proposed in [5].

The predictor for the indicator function f can be incorporated in this framework by rewriting it in conservation form using the mass conservation equation of the Euler equations. This leads to the following evolution equation for f

$$\frac{\partial}{\partial t}(\rho f) + \frac{\partial}{\partial x}(v \rho f) = 0, \quad (3.24)$$

we underline that this equation is *only* used for the predictor step and *not* for the final evolution of the numerical solution of f , which is computed by the path-conservative DG scheme (3.17).

The new ADER time-evolution procedure (3.23) evolves the piecewise polynomial data given by the WENO reconstruction or the path-conservative DG scheme for the indicator function during one time step. A time-accurate local time stepping can be derived using the one-step formulation of the finite volume and the discontinuous Galerkin schemes, (3.1) and (3.17), respectively. Due to the more restrictive time constraint of the DG scheme, a local evolution for the indicator equation is necessary. The coupling between the FV and DG methods is based on the local space-time Galerkin predictor (3.23). The basic idea is to advance the solution of the indicator function and the solution of the Euler equations in time using *different* time steps for both different numerical methods. The algorithm consists of advancing the Euler equations using a *larger* time step than the one needed by the DG scheme for the evolution of the indicator function. To synchronize the evolution of the indicator function with the evolution of the Euler equations, we adjust the DG time step by defining an integer n so that the DG time step restriction is satisfied and the following relation holds:

$$\Delta t_{FV} = n \Delta t_{DG}. \quad (3.25)$$

The local time stepping scheme permits us to exploit the full capacity of the new high order approach using the sub-cell resolution of the DG scheme to track accurately the material interfaces, but it avoids the restriction of the time step for the finite volume scheme used for the solution of the Euler equations. This robust technique not only improves the computational efficiency of the method, but also it does not need to introduce numerical diffusion in the finite volume scheme for the solution of the Euler equations. Moreover, the application of the local time stepping looks promising for the future extension to three-dimensional problems with a significant speed-up of the computation without compromising the accuracy of the results.

3.5 Sketch of the numerical scheme

In the following, we summarize the necessary steps of the algorithm described before:

1. Definition of the state in the ghost cells

Use the approximate-state Riemann solver described in Appendix to assign the states of the ghost fluid. Once the scalar nonlinear algebraic equation is solved via iteration at each interface, one assigns the computed state as the *cell average* of the ghost cells inside the three reconstruction stencils, necessary for the WENO reconstruction algorithm.

2. Reconstruction

Apply the WENO reconstruction to the Euler equations, see Section 3.2, to compute higher order polynomial data within each spatial cell at the beginning of the global time step.

3. ADER time integration with local time stepping

Using the ADER time integration update each fluid separately for one global time step as well as the indicator function for the sub-time steps, see Section 3.4. We underline that the fluid velocity v in the advection equation of the indicator function f is known from the predictor solution of the local space-time Galerkin scheme applied to the Euler equations inside each element and valid for the entire global time step of the finite volume scheme.

4. Localization of the material interface

Update the position of the interface using the values of the indicator function that defines which of the fluid states (fluid 1 or fluid 2) is valid at each grid point. The valid one is taken and the other is discarded (considered as ghost fluid from now on) so that only one real fluid is defined at each grid point.

4 Numerical results

Several test cases have been implemented to assess the accuracy of the high order scheme proposed in this paper. In some of the test cases, the incident shock wave impinging on the material interface is very strong and the original ghost fluid method does not behave well under these circumstances. All computations have been carried out using a CFL number of 0.9 and 100 cells. Only the blast-wave interaction problem of Woodward and Colella [38] has been solved with 400 cells, due to the complex structure of the solution that needs more cells to be reproduced accurately. If not mentioned otherwise, for the following test cases the one-dimensional computational domain is 1m long and the values of pressure, density, velocity and output time are given in MPa, kg/m³, km/s and ms, respectively.

4.1 Shock tube problems

We consider a modification of the well-known Sod test problem (test 1), solved also by Fedkiw et al. [15] and Hu et al. [21]. Two ideal gases with different γ are involved. The initial condition is given by

$$(\rho, v, p, \gamma) = \begin{cases} (1, 0, 1, 1.4), & \text{if } 0 < x \leq 0.5, \\ (0.125, 0, 0.1, 1.667), & \text{if } 0.5 < x \leq 1. \end{cases} \quad (4.1)$$

Transmissive boundary conditions are applied and the final output time is $t = 0.2$. The results are displayed in Fig. 1. They refer to density, velocity, total energy and pressure and show a very good agreement with the exact solution. The material interface in the density and the total energy profile is resolved sharply, as expected in a sharp-interface method, and it is also located in the correct position. Note that a very high level of accuracy is reached despite using only 100 cells and the pressure keeps constant across the material interface, without any spurious oscillations. For this test case, we note that

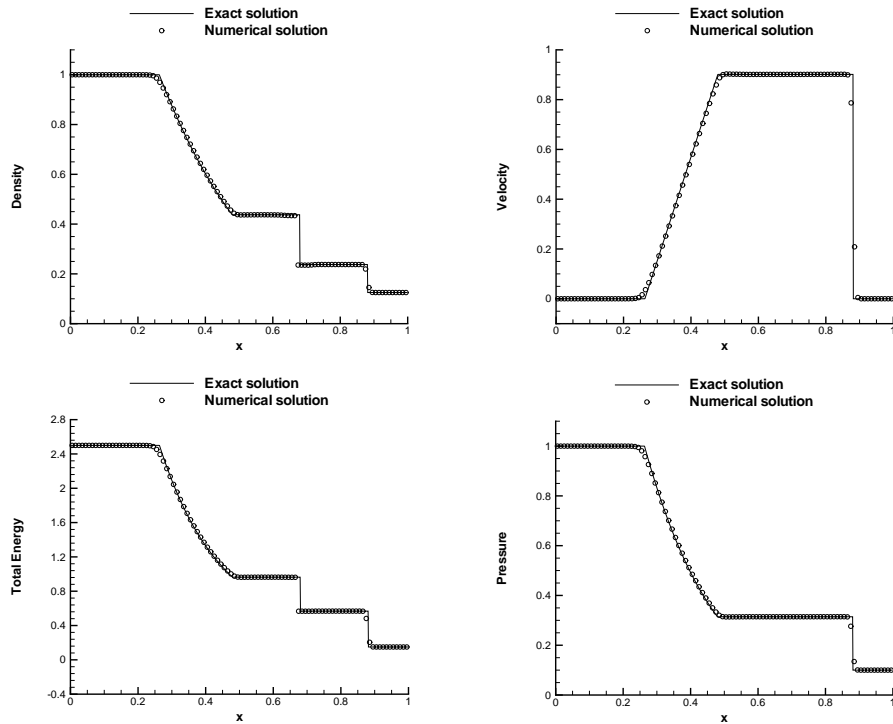


Figure 1: Numerical (symbol) and exact (line) solution of test 1 are compared at the output time $t=0.2$. The results report the density, velocity, total energy and pressure fields.

using a global time stepping scheme would have led to a total number of time steps that is *three times more* than the one of the present local time stepping algorithm. This is due to the fact that the DG scheme, used for the evolution of the indicator function induces a much more severe restriction on the time step than the finite volume scheme used for the solution of the Euler equations.

In test 2 proposed by Abgrall and Karni [2] and Hu et al. [21], the shock is very strong. Two ideal gases are involved and the initial condition consists of two constant states on the left and on the right of the material interface, as follows:

$$(\rho, v, p, \gamma) = \begin{cases} (1, 0, 500, 1.4), & \text{if } 0 < x \leq 0.5, \\ (1, 0, 0.2, 1.667), & \text{if } 0.5 < x \leq 1, \end{cases} \quad (4.2)$$

and transmissive boundary conditions have been applied. The results plotted in Fig. 2 refer to the output time $t=0.015$ computed on a mesh of 100 cells. A good agreement with the analytic solution is achieved. A sharp discontinuity at the material interface is computed in the density field. Nevertheless, a glitch appears, even when the code runs on a finer mesh of 400 cells, see Fig. 3. This is also evident in the numerical solution computed by Hu et al. [21] using 200 cells. In Fig. 2 (on the top, on the right), it is plotted the comparison between two numerical profiles of the density field obtained using two different

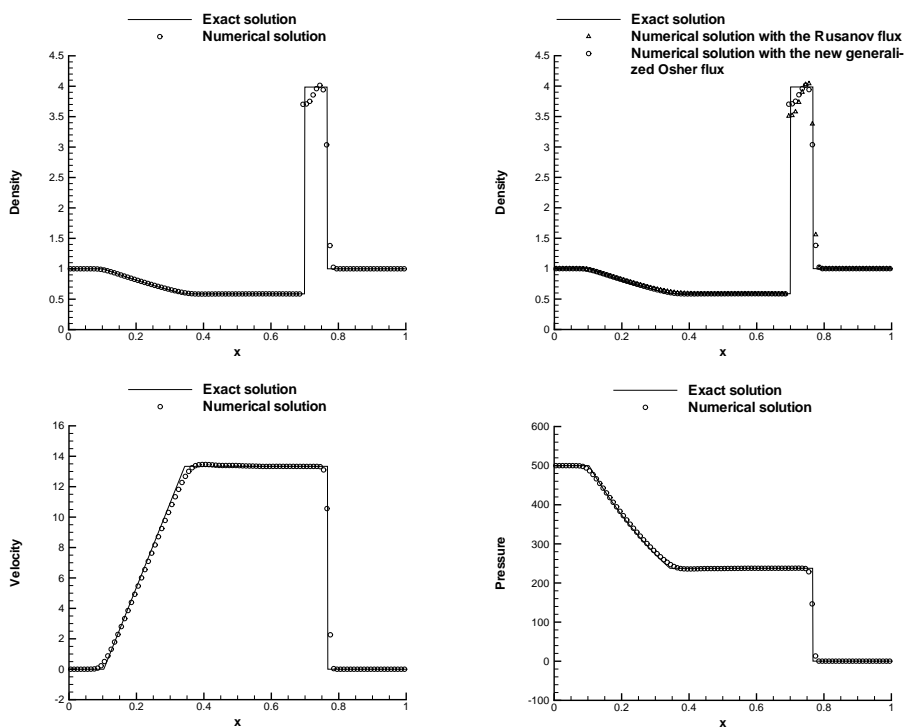


Figure 2: Numerical (symbol) and exact (line) solution of test 2 are compared at the output time $t=0.015$. In the plots the density, velocity and pressure fields are reported. On the top, on the right a comparison between the density solutions computed using the generalized Osher flux [13] (circle) and the classical Rusanov flux (triangle) is plotted. On the bottom, the solutions computed on a mesh with different resolution (100 and 400 cells) are plotted to demonstrate the convergence.

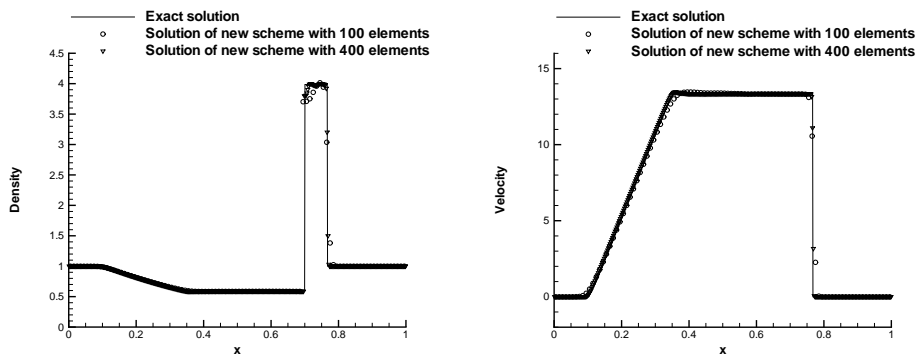


Figure 3: Numerical (symbol) and exact (line) solution of test 2 are compared at the output time $t=0.015$. The density and velocity fields are reported. The numerical solutions are computed on a mesh with different resolution, i.e., 100 and 400 cells.

fluxes, namely the classical Rusanov flux and the generalized Osher flux proposed by Dumbser and Toro [13]. The glitch at the interface becomes stronger using the Rusanov flux. This explains our choice to implement the generalized Osher flux that computes

accurate solutions. The shock located near the end of the domain (close to $x=0.8$) as well as the rarefaction wave are well solved. Fig. 3 shows the convergence of the numerical solution to the exact one when the mesh is refined. The shock and the rarefaction waves are well resolved though in spite of the glitch in the density profile.

4.2 Shock interface problems

A strong shock impacting on a gas-gas interface is computed in test 3. The incident shock wave is partly transmitted into the other fluid and partly reflected at the interface. The initial condition is

$$(\rho, v, p, \gamma) = \begin{cases} (0.384, 27.077, 100, 1.4), & \text{if } 0 < x \leq 0.2, \\ (1, 0, 1, 1.4), & \text{if } 0.2 < x \leq 1. \end{cases} \quad (4.3)$$

In this test case, the ideal gases involved have the same ratio of specific heats. The output time is equal to $t=0.03$. Transmissive conditions are applied at the boundaries. The plots in Fig. 4 show the numerical results computed on a mesh of 100 cells using the new high order scheme proposed in this paper compared against the analytic solution and the profiles obtained applying the classical ghost fluid approach of Fedkiw et al. [15]. A considerable improvement in the accuracy of the solution appears using our new high order scheme. The classical ghost fluid method fails in computing the propagation of the shocks and the material interface. A very thorough research on this topic has been carried out by Liu et al. [25] and the problems evident in the classical ghost fluid approach are essentially due to the incorrect assignment of the ghost fluid states at the material interface. Liu et al. [25] proposed to assign the ghost fluid state by a two-shock approximate state Riemann solver instead of just copying velocity and pressure and extrapolating entropy from the real fluid, as in the original ghost fluid approach.

In this article, we adopt the same strategy as the one proposed by Liu et al., however with a much simpler formulation, as can be seen in the Appendix. From the results depicted in Fig. 4, we conclude that our algorithm properly computes the correct propagation speed of discontinuities and locates the interface with a sharp jump in the density and total energy. The shocks are also resolved with a very good level of accuracy using at most three points and. In the pressure field, no spurious oscillations at the interface appear. A mesh refinement using 400 cells has been carried out to verify the convergence of the numerical solution to the exact one. The results related to the density and the velocity fields are plotted in Fig. 5. As expected, the mesh refinement yields an improvement in the resolution. Table 1 reports the CPU time required to compute test 3 using the original ghost fluid method and the new high order scheme. For both computations the third order one-step ADER time integration has been used as well as the local time stepping described in Section 3. The approximate-state Riemann solver needs a computational overhead in comparison with the original ghost fluid approach. Nevertheless, from the CPU timings reported in Table 1 the additional effort is negligible. Essentially, this is given by two reasons: the solution of the two wave approximate-state Riemann solver is

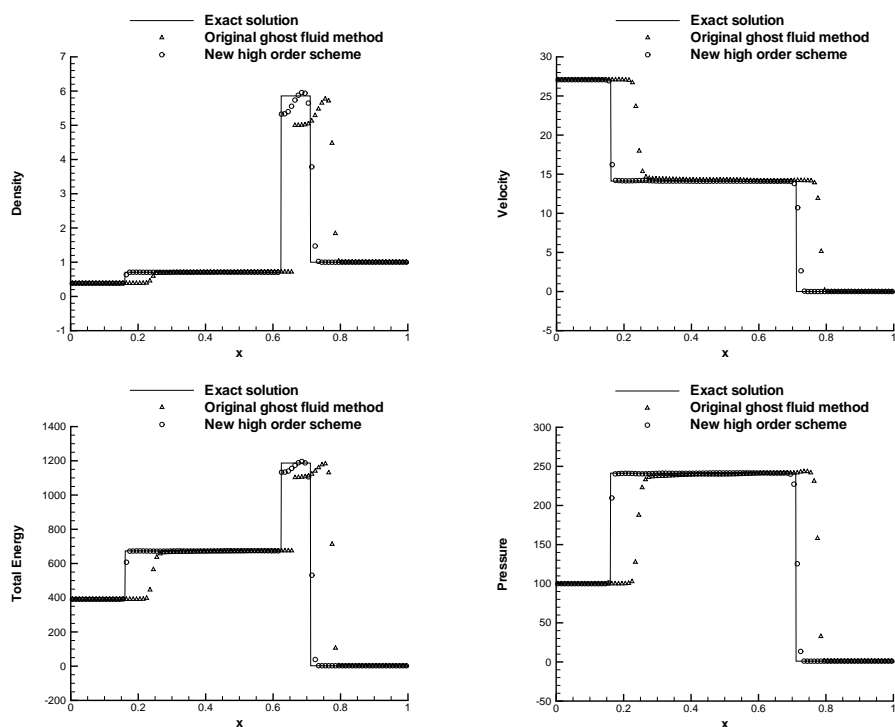


Figure 4: Numerical solutions of test 3 computed with the new high order scheme (circle) and the original ghost fluid method of Fedkiw et al. [15] (triangle) are compared against the exact solution (line) at the output time $t=0.03$. In both computations the WENO reconstruction and the third ADER time integration with local time stepping have been used on a mesh of 100 cells.

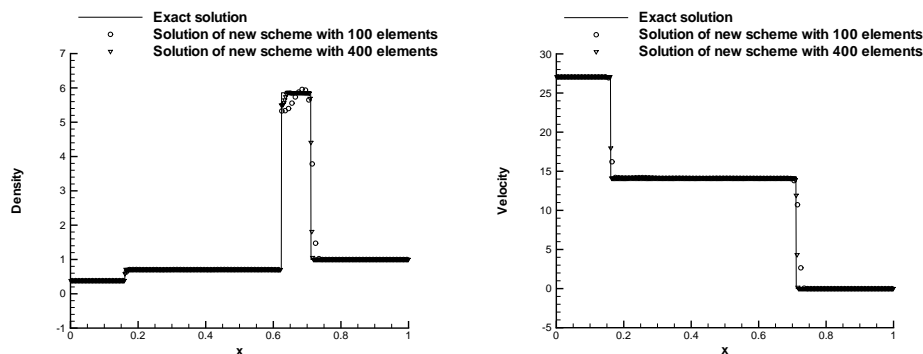


Figure 5: Numerical (symbol) and exact (line) solution of test 3 are compared at the output time $t=0.03$. The density and velocity fields are reported. The numerical solutions are computed on a mesh with different resolution, i.e., 100 and 400 cells.

efficiently solved after few iterations and a lower number of time steps have to be computed by our new high order scheme till the output time. This reduces the local overhead of CPU time due to the introduction of the approximate-state Riemann solver, especially when a large number of cells are used. From Table 1, the new high order scheme pro-

Table 1: Quantitative CPU time comparison between the original ghost fluid method (above) and the new high order scheme (below) to compute test 3. The number of cells and iterations, the total CPU time as well as the CPU time per element update for both schemes are reported.

Cells	Iterations	CPU time [s]	CPU time per element update [s]
100	166	1.14	6.86×10^{-5}
1000	1644	106.56	6.48×10^{-5}
10000	16376	10526.06	6.43×10^{-5}

Cells	Iterations	CPU time [s]	CPU time per element update [s]
100	164	1.12	6.85×10^{-5}
1000	1633	106.00	6.49×10^{-5}
10000	16328	10496.73	6.43×10^{-5}

vides a better performance at the final output time and it is definitely worth to use the approximate-state Riemann solver at the material interface.

The next challenging test case consists of the well-known blast wave problem of Woodward and Colella [38]. One ideal gas is involved and two contact discontinuities are initially located close to the boundaries of the computational domain. The initial condition is

$$(\rho, v, p, \gamma) = \begin{cases} (1, 0, 1000, 1.4), & \text{if } 0 < x \leq 0.1, \\ (1, 0, 0.01, 1.4), & \text{if } 0.1 < x \leq 0.9, \\ (1, 0, 100, 1.4), & \text{if } 0.9 < x \leq 1. \end{cases} \quad (4.4)$$

Reflective boundary conditions have been applied. The numerical solution plotted in Fig. 6 has been computed until the output time of $t=0.038$ using 400 cells. The numerical reference solution, which we consider the "exact" solution, has been obtained solving the one-phase Euler equations with a second order MUSCL-type TVD finite volume scheme with a minmod limiter and the Godunov flux based on the exact Riemann solver on a very fine mesh of 100,000 cells. In Fig. 6, a good agreement can be observed. The numerical profile reproduces well the complex structure of the solution. Two peaks in the density, velocity and total energy are computed close to $x=0.65$ and $x=0.8$. They derive from the two colliding blast waves. Both material interfaces move in time during the computation and keep sharply defined.

4.3 Gas-water interaction problems

We consider the interactions between gas and water, modeled with the ideal gas and the Tait equation of state, respectively. In this gas-water shock tube problem taken from Hu et al. [21], the initial condition is given by two constant states on each side of the material interface, as follows

$$(\rho, v, p, \gamma) = \begin{cases} (0.01, 0, 1000, 2), & \text{if } 0 < x \leq 0.5, \\ (1, 0, 1, 7.15), & \text{if } 0.5 < x \leq 1. \end{cases} \quad (4.5)$$

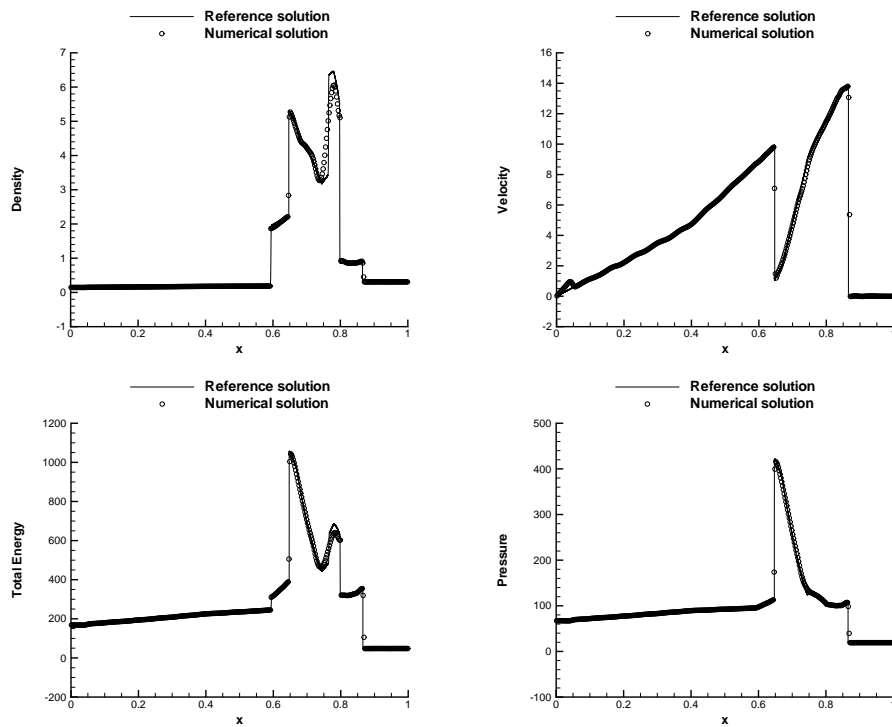


Figure 6: The numerical profiles of test 4 computed with the new high order scheme (symbol) are compared against the exact solution (solid line) at the output time $t = 0.038$. The plots refer to the profiles of density, velocity, total energy and pressure.

Transmissive conditions are applied to the boundaries. The parameters in the Tait EOS (2.5) are $k_0 = 3310$, $\rho_0 = 1$ and $p_0 = 1$. The output time is $t = 0.0008$. Fig. 7 shows the density and pressure fields computed with the new high order scheme on a mesh of 100 cells. The results show a good agreement with the exact solution. Initially, a huge jump in the pressure field is located at the interface. The high pressure region progressively expands from the gas (on the left) to the water (on the right) phase producing a shock wave. A faster reflected wave front moves to the left in the ideal gas. The material interface keeps sharply defined (about $x = 0.5$) without producing wiggles in the pressure field.

The next test case has been proposed by Liu et al. [25] and Hu et al. [21] and it consists of an air bubble collapse problem in one dimension. The initial condition is

$$(\rho, v, p, \gamma) = \begin{cases} (1.0376, 6.0151, 1000, 7.15), & \text{if } 0 < x \leq 0.7, \\ (0.001, 0, 1, 1.4), & \text{if } 0.7 < x \leq 1, \end{cases} \quad (4.6)$$

where water is on the left and ideal gas is on the right of the interface. Transmissive boundary conditions have been implemented. The parameters for the Tait EOS are given by $k_0 = 3310$ and $\rho_0 = 1$. The value of p_0 results directly from the initial condition. The final time is equal to $t = 0.003$. The numerical results are displayed in Fig. 8, that gives the density and pressure profiles. A good agreement with the analytic solution is achieved.

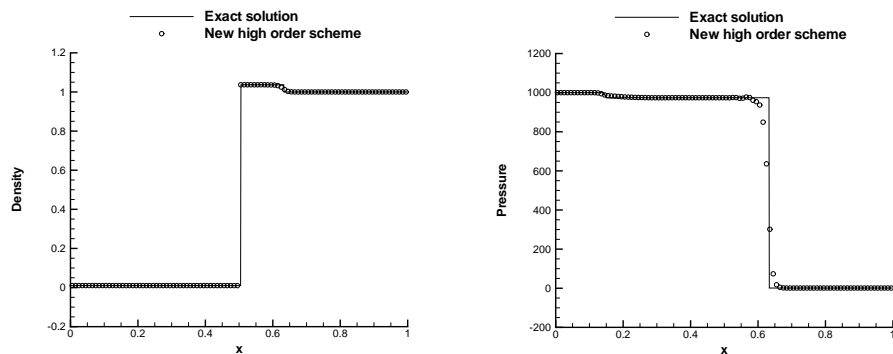


Figure 7: The numerical solution of test 5 computed with the new high order scheme (symbol) on a mesh of 100 cells is compared against the exact one (line) at the output time $t=0.0008$. The results show the interactions between an ideal gas, on the left, and water, on the right of the material interface.

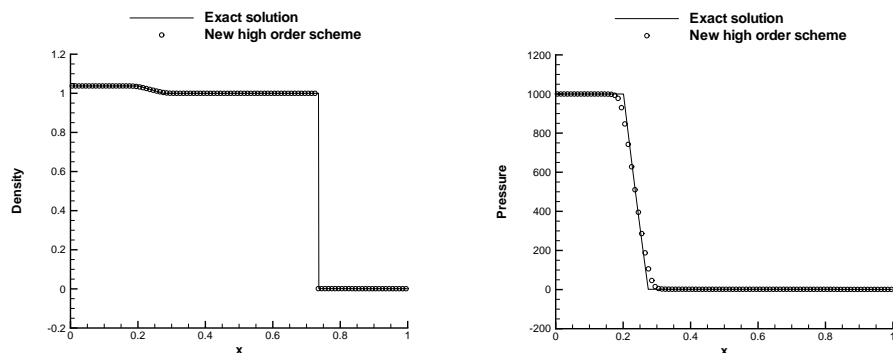


Figure 8: The numerical solution of test 6 computed with the new high order scheme (symbol) on a mesh of 100 cells is compared against the exact one (line) at the output time $t=0.003$. The results show the interactions between water, on the left, and an ideal gas, on the right of the material interface.

The material interface is sharply defined, as shown in the density profile in Fig. 8, on the left. In this case, the high pressure value is initially into water, on the left. Instead of a shock, the pressure jump across the interface produces a rarefaction wave that moves to the left, decreasing the density of water and the related pressure value.

4.4 Low Mach number problems

Now we consider the limit case when the Mach number tends to zero and hence the compressible Euler equations tend to the incompressible ones. The propagation rate of the pressure waves becomes infinite and the equations change their type (from hyperbolic to hyperbolic-elliptic). In our applications, we approach the incompressible behavior by simulating a weakly compressible fluid at low Mach number using the Tait equation of state in the compressible Euler equations.

A non-trivial example consists of a one-dimensional test case proposed by Munz et al. [28]. An acoustic wave is generated by the time-dependent boundary values for the

velocity, as follows

$$v(a,t) = +M_B \sin(t), \quad v(b,t) = -M_B \sin(t), \quad M_B = 0.0025, \quad \text{for } t \in \mathbb{R}_0^+, \quad (4.7)$$

where M_B denotes the Mach number related to the boundary conditions, a and b are the boundaries of the spatial interval $I = [a,b] = [0,\pi]$. A single-phase fluid is located inside the domain

$$(\rho, v, p, \gamma) = \left\{ \left(1, 0, \frac{1}{\gamma}, 1.4 \right), \quad 0 < x < \pi \right\}. \quad (4.8)$$

The output time is equal to $t = 2$. The parameters of the Tait equations consists of $\rho_0 = 1$ and $p_0 = 1/\gamma$. The value of k_0 can be derived from Eq. (2.5) assuming the maximum value of the fluid speed equal to $|v| = 0.0025$. The non-trivial analytic solution of the problem denoted by $(\rho^{AS}, v^{AS}, p^{AS})$ has been obtained by Munz et al. [28] solving the Euler equations in the limit $M \rightarrow 0$. It reads

$$\rho^{AS}(x,t) = A \left(\cosh\left(\frac{2M}{\pi}\right) - \sinh\left(\frac{2M}{\pi}\right) \right), \quad (4.9a)$$

$$v^{AS}(x,t) = M \sin(t) \left(1 - \frac{2x}{\pi} \right), \quad (4.9b)$$

$$p^{AS}(x,t) = \frac{1}{\gamma} - \frac{2M(\cos(t)-1)}{\pi} + M^2 AB (\pi \cos(t) + M(\cos(2t)-1)) \frac{x(x-\pi)}{\pi^2}, \quad (4.9c)$$

where the terms A and B are defined as follows:

$$A = e^{-\frac{2}{\pi} M \cos(t)}, \quad (4.10a)$$

$$B = \sinh\left(\frac{2M}{\pi}\right) + \cosh\left(\frac{2M}{\pi}\right). \quad (4.10b)$$

In Fig. 9, the density and the velocity field are displayed. The plots report the analytic solution and the numerical solutions computed on a mesh of 100 cells using a global Mach number of $M = 0.0025$ and $M = 0.00025$. As expected, reducing the Mach number, the numerical solution converges to the incompressible behavior: the oscillations in the density field are drastically reduced and the velocity profile follows well the linear exact solution.

In the next test case we analyze the interactions between water and gas, when two shock waves come from the boundaries. A drop of water is located in the middle of the domain and it is modeled as a weakly compressible fluid with a low Mach number. The initial condition is given by

$$(\rho, v, p, \gamma) = \begin{cases} (1.225, 0, 101325, 1.4), & \text{if } 0 < x \leq 0.4, \\ (1000, 0, 101325, 7.15), & \text{if } 0.4 < x \leq 0.6, \\ (1.225, 0, 101325, 1.4), & \text{if } 0.6 < x \leq 1. \end{cases} \quad (4.11)$$

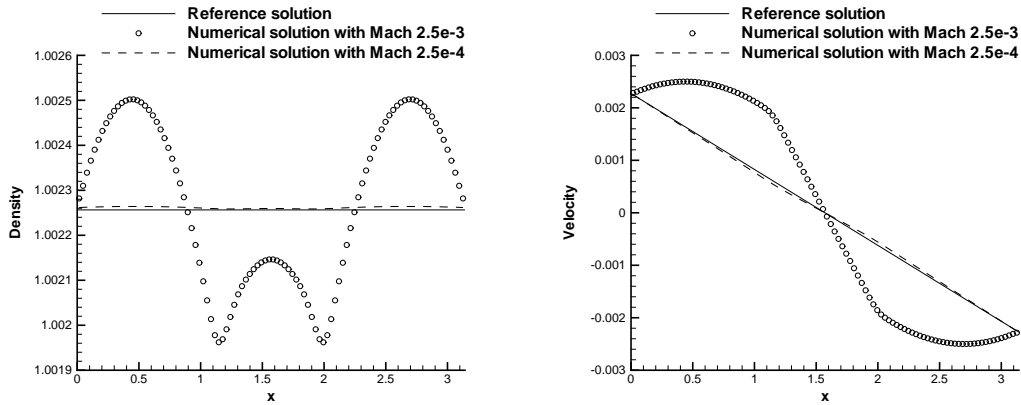


Figure 9: The numerical solutions of test 7 computed with a global Mach number of $M=0.0025$ (symbol) and $M=0.00025$ are compared against the exact one (solid line) at the output time $t=2$. Both computations have been carried out using the new high order scheme on a mesh of 100 cells. The results show the density and velocity fields.

The values of pressure and velocity are given in Pa and m/s, respectively. The computational domain is 1cm long. The boundary condition generates high constant compression that propagates from the boundaries into the domain

$$v(a,t) = +v_B, \quad v(b,t) = -v_B, \quad v_B = 360, \quad \text{for } t \in \mathbb{R}_0^+, \quad (4.12)$$

where a and b are the boundaries of the spatial interval

$$I = [a,b] = [0,1]. \quad (4.13)$$

The computation has been carried out using 201 cells. The parameters for the Tait equation of state are $\rho_0 = 1000$, $p_0 = 101325$ and k_0 is obtained from Eq. (2.5) with a Mach number of $M = 0.025$. Fig. 10 shows the numerical velocity and the pressure fields at time $t = 0.01, 0.03$ and 0.035 . To have clearer plots, the gas phase is denoted by cross and water by circle. At the first output time the shock waves from the boundaries have reached the water drop and they have been reflected at the interface. The high compression perturbs the pressure field in the drop that assumes a parabolic profile, similar to the analytic solution p^{AS} (4.9c) of the previous test case. The numerical solution for water shows a quasi-linear velocity distribution and this is true for all time steps, see the zoom regions in Fig. 10. Again, this is convalidated by the analytic velocity field v^{AS} in Eq. (4.9b), related to the low Mach number problem above. At time $t = 0.03$, the shocks have been reflected for the second time at the interface. The pressure increases in the gas phase as well as in the liquid phase. Again a parabolic pressure profile in the drop has been obtained. After, at time $t = 0.035$, the amplified shock waves are coming to the drop interfaces and the curvature of the pressure profile in water changes again. These pressure oscillations in the drop are due to the dynamics of the problem that introduces an increasing compression from the boundaries.

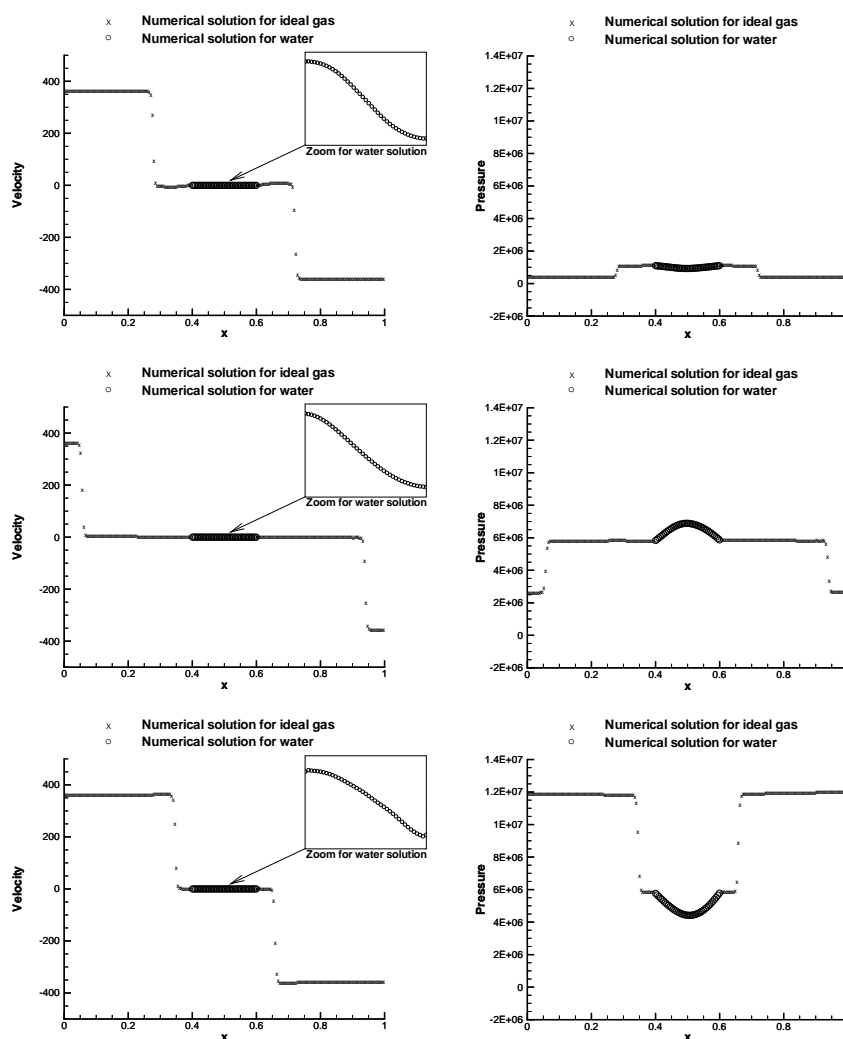


Figure 10: The numerical solutions of the velocity and pressure fields related to test 8 at the output time $t=0.01, 0.03$ and 0.035 . The computation has been carried out using 201 cells and a Mach number of $M=0.025$ for water. The gas phase is denoted by cross and water by circle.

5 Conclusions and future work

In this paper, we have proposed a new high order scheme that combines a path-conservative approach applied to the DG scheme for the discretization of the indicator function, with the high order WENO FV method for the discretization of the Euler equations. Moreover, applying a high order ADER-type one-step procedure for the time discretization, time-accurate local time steps have been used to improve the numerical accuracy and the computational performance of the method.

Many of the numerical tests proposed in literature [2, 21, 25, 28] have been solved.

Good accuracy and performance have been assessed, despite using a rather coarse mesh of only 100 points. This is due to the high order of accuracy of the scheme, that exploits the sub-cell resolution of the DG scheme to track the material interface, the high accuracy of the new generalized Osher flux proposed by Dumbser and Toro [13] and the new approximate-state Riemann solver used to assign the states to the ghost cells.

Future work will concern the extension of our new numerical approach for compressible multi-phase flows to multi-dimensions based on the encouraging results in 1D published in this paper. Our purpose is also to compare future results with other completely different computational approaches, such as the 3D Lagrangian smooth particle hydrodynamics (SPH) method proposed by Ferrari et al. [16, 17] to validate our Eulerian ghost fluid scheme.

Acknowledgments

The authors would like to acknowledge the support by the Deutsche Forschungsgemeinschaft (DFG) in the framework of the collaborative research project SFB-TRR 40 and the Cluster of Excellence "Simulation Technology" (SimTech).

Appendix: Two wave approximate-state Riemann solver for phase interactions

To compute the interactions across the material interface, we use the ghost fluid approach, originally proposed by Fedkiw et al. in [14, 15]. The new idea published in this paper is about how to compute the state in the ghost cells. Instead of solving a system of six nonlinear algebraic equations like Liu et al. [25], we reduce the problem to one simple scalar nonlinear algebraic equation, thus improving considerably the computational efficiency. We apply an approximate-state Riemann solver that consists of a two-shock approximation for the gas phase, modeled with ideal gas EOS and a two-rarefaction approximation for water, modeled with the Tait EOS. For details on the complete exact Riemann solver, see [35]. It provides the solution of the Riemann problem at the material interface via iteration after some steps solving the following scalar nonlinear algebraic equation

$$g_L + g_R + \Delta v = 0, \quad \Delta v = v_R - v_L, \quad (\text{A.1})$$

where the indexes L and R denote the left and the right side at the interface. The function g and its derivative ∂g (needed by the Newton method) are defined as follows:

$$g_S = \begin{cases} \frac{2}{\gamma-1} c_S \left[\left(\frac{p}{p_S} \right)^{\frac{\gamma-1}{2\gamma}} - 1 \right], & \text{for ideal gas,} \\ \frac{2}{\gamma-1} (c - c_S), & \text{for water,} \end{cases} \quad (\text{A.2})$$

$$\partial g_S = \begin{cases} \frac{1}{\rho_S c_S} \left(\frac{p}{p_S} \right)^{-\frac{\gamma+1}{2\gamma}}, & \text{for ideal gas,} \\ \frac{c}{\rho}, & \text{for water,} \end{cases} \quad (\text{A.3})$$

where the index S is introduced to indicate the left or the right state at the interface, so that $S = L, R$, and c is the sound speed related to each phase. The solution of Eq. (A.1) provides the state at the interface, that is one value of velocity and the pressure and two values of density, each of them related to the phases. For initial guess values, we have taken the average state between the left and the right side of the material interface. A more sophisticated procedure for obtaining a good initial guess is described in [35]. Convergence is obtained very quickly by a standard Newton method.

References

- [1] R. Abgrall, How to prevent pressure oscillations in multicomponent flow calculations: a quasi conservative approach, *J. Comput. Phys.*, 125 (1996), 150–160.
- [2] R. Abgrall and S. Karni, Computations of compressible mult fluids, *J. Comput. Phys.*, 169 (2001), 594–623.
- [3] C.-H. Chang and M.-S. Liou, A robust and accurate approach to computing compressible multiphase flow: stratified flow model and AUSM \ddagger -up scheme, *J. Comput. Phys.*, 225 (2007), 840–873.
- [4] B. Cockburn and C. W. Shu, The Runge-Kutta discontinuous Galerkin method for conservation laws V: multidimensional systems, *J. Comput. Phys.*, 141 (1998), 199–224.
- [5] M. Dumbser, D. Balsara, E. F. Toro and C. D. Munz, A unified framework for the construction of one-step finite-volume and discontinuous Galerkin schemes on unstructured meshes, *J. Comput. Phys.*, 227 (2008), 8209–8253.
- [6] M. Dumbser, M. Castro, C. Parés and E. F. Toro, ADER schemes on unstructured meshes for nonconservative hyperbolic systems: applications to geophysical flows, *Comput. Fluids.*, 38 (2009), 1731–1748.
- [7] M. Dumbser, C. Enaux and E. F. Toro, Finite volume schemes of very high order of accuracy for stiff hyperbolic balance laws, *J. Comput. Phys.*, 227 (2008), 3971–4001.
- [8] M. Dumbser, A. Hidalgo, M. Castro, C. Parés and E. F. Toro, FORCE schemes on unstructured meshes II: non-conservative hyperbolic systems, *Comput. Meth. Appl. Mech. Eng.*, 199 (2010), 625–647.
- [9] M. Dumbser and M. Käser, Arbitrary high order non-oscillatory finite volume schemes on unstructured meshes for linear hyperbolic systems, *J. Comput. Phys.*, 221 (2007), 693–723.
- [10] M. Dumbser, M. Käser, V. A. Titarev and E. F. Toro, Quadrature-free non-oscillatory finite volume schemes on unstructured meshes for nonlinear hyperbolic systems, *J. Comput. Phys.*, 226 (2007), 204–243.
- [11] M. Dumbser, M. Käser and E. F. Toro, An arbitrary high order discontinuous Galerkin method for elastic waves on unstructured meshes V: local time stepping and p-adaptivity, *Geophys. J. Int.*, 171 (2007), 695–717.
- [12] M. Dumbser and C.-D. Munz, Building blocks for arbitrary high order discontinuous Galerkin schemes, *J. Sci. Comput.*, 27 (2006), 215–230.

- [13] M. Dumbser and E. F. Toro, A simple extension of the Osher Riemann solver to non-conservative hyperbolic systems, *J. Sci. Comp.*, in press. DOI: 10.1007/s10915-010-9400-3
- [14] R. P. Fedkiw, T. Aslam and S. Xu, The ghost fluid method for deflagration and detonation discontinuities, *J. Comput. Phys.*, 154 (1999), 393–427.
- [15] R. Fedkiw, T. Aslam, B. Merriman and S. Osher, A Non-oscillatory Eulerian approach to interfaces in multimaterial flows (the ghost fluid method), *J. Comput. Phys.*, 152 (1999), 457–492.
- [16] A. Ferrari, M. Dumbser, E. F. Toro and A. Armanini, A new stable version of the SPH method in Lagrangian coordinates, *Comm. Comput. Phys.*, 4(2) (2008), 378–404.
- [17] A. Ferrari, M. Dumbser, E. F. Toro and A. Armanini, A new 3D parallel SPH scheme for free surface flows, *Comput. Fluids.*, 38 (2009), 1203–1217.
- [18] G. Gassner, F. Lörcher and C. D. Munz, A discontinuous Galerkin scheme based on a space-time expansion II: viscous flow equations in multi dimensions, *J. Sci. Comput.*, 34 (2008), 260–286.
- [19] A. Harten, B. Engquist, S. Osher and S. Chakravarthy, Uniformly high order essentially non-oscillatory schemes, III, *J. Comput. Phys.*, 71 (1987), 231–303.
- [20] C. W. Hirt and B. D. Nichols, Volume of fluid (VOF) method for dynamics of free boundaries, *J. Comput. Phys.*, 39 (1981), 201–225.
- [21] X. Y. Hu, N. A. Adams and G. Iaccarino, On the HLLC Riemann solver for interface interaction in compressible multi-fluid flow, *J. Comput. Phys.*, 228 (2009), 6572–6589.
- [22] P. Jenny and B. Müller and H. Thomann, Correction of conservative Euler solvers for gas mixtures, *J. Comput. Phys.*, 132 (1997), 91–107.
- [23] G. S. Jiang and C. W. Shu, Efficient implementation of weighted ENO schemes, *J. Comput. Phys.*, 126 (1996), 202–228.
- [24] M.-S. Liou, A sequel to AUSM: AUSM \ddagger , *J. Comput. Phys.*, 129 (1996), 364–382.
- [25] T. G. Liu, B. C. Khoo and K. S. Yeo, Ghost fluid method for strong shock impacting on material interface, *J. Comput. Phys.*, 190 (2003), 651–681.
- [26] E. Marchandise, J.-F. Remacle and N. Chevaugeon, A quadrature-free discontinuous Galerkin method for the level set equation, *J. Comput. Phys.*, 212 (2006), 338–357.
- [27] W. Mulder, S. Osher and J. A. Sethian, Computing interface motion in compressible gas dynamics, *J. Comput. Phys.*, 100 (1992), 209–228.
- [28] C.-D. Munz, M. Dumbser and S. Roller, Linearized acoustic perturbation equations for low Mach number flow with variable density and temperature, *J. Comput. Phys.*, 224 (2007), 352–364.
- [29] S. Osher and F. Solomon, Upwind difference scheme for hyperbolic conservation laws, *Math. Comput.*, 38 (1982), 339–374.
- [30] C. Parés, Numerical methods for nonconservative hyperbolic systems: a theoretical framework, *SIAM J. Num. Anal.*, 44 (2006), 300–321.
- [31] J. Qiu, M. Dumbser and C. W. Shu, The discontinuous Galerkin method with Lax-Wendroff type time discretizations, *Comput. Method. Appl. Math.*, 194 (2005), 4528–4543.
- [32] S. Rhebergen, O. Bokhove and J. J. W. van der Vegt, Discontinuous Galerkin finite element methods for hyperbolic nonconservative partial differential equations, *J. Comput. Phys.*, 227 (2008), 1887–1922.
- [33] M. Sussman, P. Smereka and S. Osher, A level set approach for computing solutions to incompressible two-phase flow, *J. Comput. Phys.*, 114 (1994), 146–159.
- [34] V. A. Titarev and E. F. Toro, ADER schemes for three-dimensional nonlinear hyperbolic systems, *J. Comput. Phys.*, 204 (2005), 715–736.

- [35] E. F. Toro, *Riemann Solvers and Numerical Methods for Fluid Dynamics: A Practical Introduction*, 2nd. ed., Springer, 1999.
- [36] E. F. Toro and V. A. Titarev, Solution of the generalized Riemann problem for advection-reaction equations, *Proc. Roy. Soc. London. A.*, 458 (2002), 271–281.
- [37] E. F. Toro and V. A. Titarev, Derivative Riemann solvers for systems of conservation laws and ADER methods, *J. Comput. Phys.*, 212 (2006), 150–165.
- [38] P. Woodward and P. Colella, The numerical simulation of two-dimensional fluid flow with strong shocks, *J. Comput. Phys.*, 54 (1984), 115–173.